Characterization of AlCrN and AlCrON Coatings Deposited on Plasma Nitrided AISI H13 Steels Using Ion-Source-Enhanced Arc Ion Plating

Farooq Ahmad [1,2], **Lin Zhang [1,***, **Jun Zheng [1,2]**, **Iram Sidra [1,2]** and **Shihong Zhang [1,2,***

[1] Key Laboratory of Green Fabrication and Surface Technology of Advanced Metal Materials (Ministry of Education), Research Center of Modern Surface & Interface Engineering, Anhui University of Technology, Maanshan 243002, China; mrfl24@yahoo.com (F.A.); zhengj510@163.com (J.Z.); sidrairam.phy@gmail.com (I.S.)

[2] School of Materials Science and Engineering, Anhui University of Technology, Maanshan 243002, China

* Correspondence: zhanglin_dut@163.com (L.Z.); tougaoyouxiang206@163.com (S.Z.)

Abstract: The AlCrN and AlCrON coatings were deposited on plasma nitrided H13 steels through ion-source-enhanced arc ion plating, and their structures, mechanical properties, thermal stabilities, and tribological properties were investigated. Structural analysis showed that the monolayer AlCrN and AlCrON bilayered coatings were mainly composed of fcc-AlCrN and fcc-AlCrON solid solution phases respectively. Upon the addition of thin AlCrON layer, the hardness of AlCrN/AlCrON coating slightly decreased from about 30.5 GPa to 28.6 GPa, and the thermal stability was improved after annealing at 700 °C. Both coatings exhibited excellent wear resistance at room temperature, while all wear process involved a combination of wear mechanisms, including severe abrasion and oxidation at an evaluated temperature. The AlCrON bilayered coating showed better wear resistance than that of AlCrN coating due to a dense anti-oxidation layer and better adhesion at a high temperature, making it suitable for die tool protection coatings.

Keywords: microstructure; tribology; AlCrON coating; ion-source-enhanced arc ion plating

1. Introduction

High-pressure die casting (HPDC) has gained increasing attention due to its capability to allow mass production and short processing time. Regardless of the advancement in surface treatment and coating development, HPDC is still facing severe challenges, such as wear, erosion, and chemical corrosion at evaluated temperatures [1–3]. Traditional surface treatment methods cannot satisfy practical engineering requirements. The duplex physical vapor deposition (PVD) coatings combined with plasma nitriding (PN) significantly improve tool life and lower the cost per injection [4,5]. Plasma nitriding prior to deposition of a PVD coating enables improving the loading capacity of the substrate and provides proper stress and hardness gradients between the coating and the substrate, which contribute considerably to the increase in performance of the PVD coating.

Transition metal nitride coatings, such as TiN; CrN; TiN/TiAlN; binary; multilayer; and multi-component coatings—CrN/AlN/Al$_2$O$_3$, CrON, TiAlN, AlCrN, or TiAlCrN—on PN substrates were tested and evaluated in practical die-casting [4–10]. Comparatively, a Cr$_2$O$_3$ passive layer provides better protection against oxidation in a Cr-based coating compared to Ti$_2$O$_3$ in Ti-based coatings [11]. Due to the improved wear resistance and oxidation resistance, the AlCrN coatings are beneficial for tool protection at high temperatures [12,13]. Moreover, the properties of oxy-nitride coatings are greatly influenced by the incorporation of oxygen due to metallic-ionic bonds [14,15]. Several studies have discussed the incorporation of oxygen in nitride coating, and its effect on oxidation

resistance and mechanical properties [14–16]. AlCrON coatings show potential in different applications of turbine blades, plastic processing dyes, and cutting tools [17–19]. In contrast, reports also show that the incorporation of oxygen significantly deteriorates the mechanical behavior of hard coatings [20,21], making it necessary to investigate the comparative microstructural and mechanical properties of AlCrN and AlCrON coatings.

At present, AlCrN and AlCrON coatings were synthesized by different PVD technologies in different applications [18,19,22–24]. The different coating deposition technologies have some advantages and disadvantages over others, depending upon the desired properties [25]. The higher ionization rate, higher deposition rate, and lower deposition temperature of arc ion plating technology favor the deposition of hard coatings for tool protection, while the ion source pre-treatment provides comparatively lower surface roughness [26]. In this study, the AlCrN and AlCrN/AlCrON duplex coatings were prepared by ion-source-enhanced arc ion plating on PN-AISI H13 steels. This study aimed to investigate the microstructures, mechanical properties, thermal stabilities, and tribological properties of AlCrN and AlCrN/AlCrON coatings at high temperature.

2. Materials and Methods

The monolayer AlCrN and AlCrON (with AlCrN base layer) bilayered coatings were deposited on plasma nitrided AISI H13 steel substrates. The specimens were ground using SiC abrasive papers and then polished with a 2.5 μm diamond paste to the roughness of Ra lower than 0.02 μm. The specimens were cleaned in an ultrasonic cleaner with acetone and ethanol for 10 min respectively. Prior to coating deposition, all the polished specimens were plasma nitrided in a vacuum chamber at 510 °C for eight hours in a mixture of gaseous N_2 and H_2 (1:3 v/v), succeeded by slow furnace cooling. The coatings were deposited by an industrial ion-source-enhanced arc ion plating system using two AlCr alloy targets with 70 at.% Al composition. The ion-source-enhanced arc ion plating was based on the multi-arc ion plating method combined with high energy Ar ion cleaning pretreatment. During the ion source cleaning procedure, Ar gas was ionized by using a rotating cathode of Ti target with a shield plate, which created highly efficient argon etching to enhance the adhesive strength between coating and substrate. The detail process about substrate cleaning using the ion source effect was reported elsewhere [26]. Before coating deposition, the nitrided specimens substrates were preheated to 450 °C and the base pressure was kept below 1×10^{-3} Pa. The substrates were firstly sputter cleaned in Ar plasma at 4.0 Pa pressure with a bias of −400 V for 10 min, and then the ion source cleaning was performed at a substrate bias of −300 V for 30 min to etch the substrate by the high density and energy Ar ions. The monolayer AlCrN and AlCrN/AlCrON bilayered coatings were prepared using the same arc current of 140 A and substrate bias voltage of −50 V. The deposition temperature was maintained at 450 °C for both coatings. The AlCrN coating was deposited at a constant bias pressure of 3.5 Pa in a pure N_2 gaseous environment (99.999% purity) for 90 min. The second coating consisted of two layers: an AlCrN adhesion layer and the AlCrON top layer. The AlCrN base layer was deposited for 60 min using the aforementioned parameters. The AlCrON top layer was deposited under the O_2/N_2 flow ratio of 1:10 in an N_2 and O_2 mixture gaseous environment for 30 min, keeping the same constant deposition pressure of 3.5 Pa.

The surface morphology, thickness, and surface roughness of every specimen was measured using SEM (Phenom-XL, Nieuw-Vennep, Netherland), a ball crater, and the KLA-Tencor P7 step profiler (Hunnenpad, Netherland), respectively. The phase structure of duplex coatings was analyzed by X-ray diffractometer (XRD, Burkar D8 Advance, Karlsruhe, Germany), operated at 40 kV and 40 mA with radiation source Cu-kα (wavelength λ = 0.15406 nm) and a 0.02° step size; a 0.05 s dwell time was set to record a diffraction spectra in a range from 20° to 80°. The bonding states of chemical elements were characterized by an X-ray photoelectron spectrometer (XPS, Thermo ESCALAB 250, Dreieich, Germany) operated at 150 W, Al-Kα (h_v = 1486.6 eV) radiation source. The specimen surface was sputtered clean for 10 min with Ar^+ ions before obtaining the spectra. The XPS spectra were calibrated by the adventitious carbon C 1s peak at 284.6 eV. The microstructures of the coatings were

determined using a transmission electron microscope (HRTEM, FEI-F20, Tecnai, Stanford, CA, USA). The cross-sectional microstructure of the coating was observed after preparing the specimen with end milling by a focus ion beam (FIB) system operated at 4.5 Kev and an incident angle of 3°–8°.

The surface hardness values and elastic moduli of duplex coatings were determined by nano-indentation tests under a loading rate of 40 mN·min^{-1} and a dwell-time of 15 s. The substrate influence was reduced using a maximum load of 25 mN so that the penetration depth was less than 10% of the coating thickness. A standard Rockwell-C indentation tester with a load of 1470 N was employed to evaluate the adhesion strength of each duplex coating, and SEM was used to observe the indentation impresses. To investigate the thermal stability, the as-deposited coatings were simultaneously annealed in a nitrogen gas environment in a resistive furnace. The annealing was performed at 700 °C for 6 h at the uniform heating rate of 5 °C/min. The effects of annealing on the structural evolutions of coatings were analyzed by XRD and Raman spectroscopy. A micro-Raman spectrometer (InVia, Renishaw, Alcester, UK) with a 514 nm argon-ion laser as the excitation source was used to obtain the Raman spectra from the as-deposited and post-annealing surfaces.

The wear behavior of each duplex coating was evaluated using a ball-on-disk tribometer at room temperature (RT) and 600 °C (HT), respectively. The Al$_2$O$_3$ ball of 6 mm diameter was used as a counterpart for wear tests with the following test parameters: a 5 N load, a 0.25 m/s speed, and a 1 h sliding time. A computer connected to the ball-on-disk apparatus records the variations in the ratio between tangential force and normal force and returns the coefficient. The step profiler and SEM were used to analyze the worn tracks of the coatings. The results of wear rates on coatings were calculated based upon a modified Archad's wear model [27].

3. Results and Discussion

3.1. Coating Morphologies

The surface morphologies of as-deposited coatings are shown in Figure 1. The SEM images in Figure 1a,b present several macroparticles on the coating surface, which is a common characteristic of the arc evaporation process due to the high ionic current density of arc sources. The density and sizes of macroparticles in a AlCrON coating are greater compared to an AlCrN coating. The 3D surface morphology of the coatings was measured by step profiler, as shown in Figure 1c,d. The average surface roughness of *S*a = 0.108 ± 0.005 μm for an AlCrN coating is lower than for an AlCrON coating—*S*a = 0.129 ± 0.006 μm—which is obvious in oxynitride coatings because of target poisoning in a conventional arc deposition process. This can be related to the presence of oxygen in the deposition chamber; oxygen reacts with a freshly exposed target surface and forms a passive oxide zone. The active region on the target surface becomes smaller and increases the arc current density, resulting in the ejection of larger particles and the formation of solid agglomerates on the coated surface [28,29]. The coating thicknesses were about 3.5 and 3.2 μm for AlCrN and AlCrON bilayered coatings respectively, which showed the reduction of deposition rate with the introduction of oxygen. The reduction in the rate of deposition can be attributed to the oxygen content, which leads to the preferred reaction of aluminum and oxygen, and thence the premature formation of non-conductive layers on the targets [22].
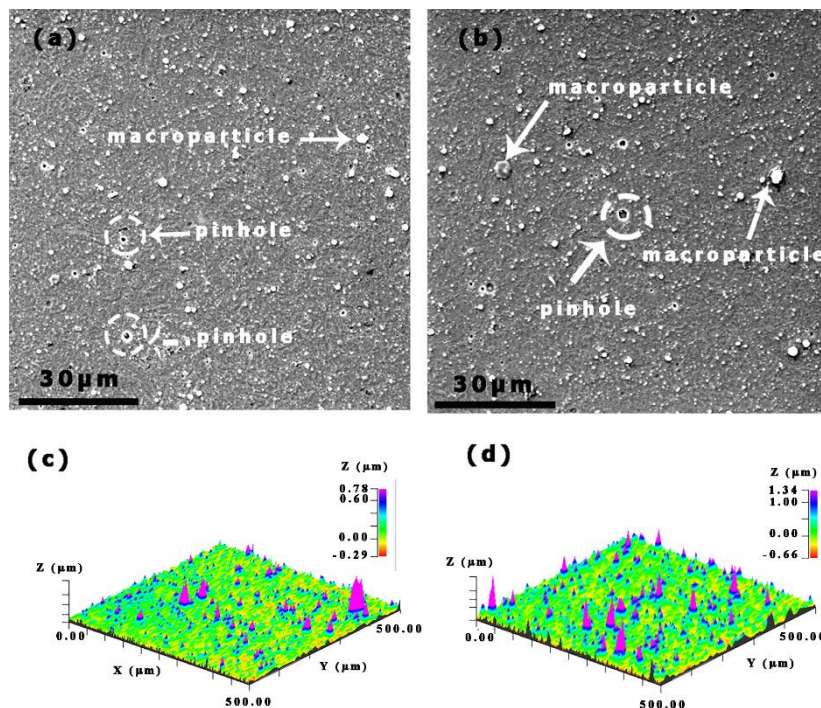
Figure 1. The surface morphologies of as-deposited coatings: (**a**) SEM image of AlCrN; (**b**) SEM image of AlCrON; (**c**) 3D surface morphology of AlCrN; (**d**) 3D surface morphology of AlCrON.

3.2. Microstructure Analysis

Figure 2 shows the XRD pattern of as-deposited AlCrN and AlCrON coatings. The AlCrN coating mainly consists of a rock salt type cubic structure with peaks at $2\theta = 37.5°, 43.6°$, and $63.5°$ corresponding to (111), (200), and (220) fcc-CrN (JCPDS# 11-0065), respectively [15]. The most dominant peaks with (111) preferential orientation can be assigned to CrN and c-AlN (JCPDS# 25-1495), The relative peaks positioned in between CrN and c-AlN can be attributed to the formation of the fcc-(Cr, Al)N solid solution phase [30,31]. The increase in the intensity of the (200) diffraction peak grew with the introduction of oxygen, which indicated the growth of plans with lower surface energy [29]. Moreover, the apparent change in the shape of (200) peak observed in the diffraction spectra can be related to the compressive residual stress, and structural defects resulting from the replacement of N^{3-} ions by O^{2-} ions in the charge balancing mechanism and the disordered distribution of Al and Cr ions on metal sites. The structural defects such as vacancies on metal sites were due to the charge balance mechanism in oxynitride coatings [14,15].

X-ray photoelectron spectroscopy was employed to investigate the bonding structures of AlCrN and AlCrON duplex coatings. Figure 3a presents the Cr 2p3/2 band, and its two de-convoluted peaks located at 575.3 and 577.3 eV correspond to CrN and Cr_2O_3 respectively [32]. Figure 3b shows the decomposed spectra of Al 2p. Two peaks located at 73.8 and 74.4 eV were assigned to AlN and Al_2O_3 [32,33]. In Figure 3c, the N 1s spectra reveal the presence of CrN and AlN at 396.3 and 397.2 eV respectively [32]. In Figure 3d, the O 1s spectra indicate the Cr_2O_3 and Al_2O_3 bonding states at 530.8 and 531.5 eV respective binding energies [32].

The bonding fractions Cr-N, Cr-O, Al-N, and Al-O of AlCrN and AlCrON coatings were compared to investigate the influence of oxygen in the chemical bond evolution process. The Cr-N bond fraction reduced from 61.5% to 6%, and the Al-N bond fraction decreased from 63% to 7.5% in AlCN and AlCrON coatings respectively. Correspondingly, the Cr-O band fraction improved from 39.5% to 94% and the Al-O bond fraction enhanced from 37% to 92.5% in AlCrN and AlCrON coatings respectively. The oxygen bond fraction in AlCrN coating was present possibly due to residual surface impurities and an organic substance in a vacuum chamber. Based on the XPS results, it was confirmed that the

AlCrON solid solution phase mainly formed in thin AlCrON top layer, which was consistent with XRD results.
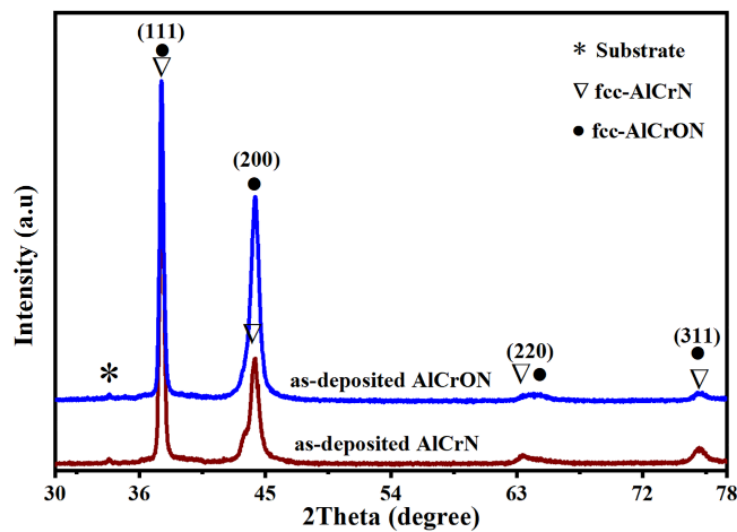
Figure 2. XRD patterns of the AlCrN and AlCrON duplex coatings for steel.
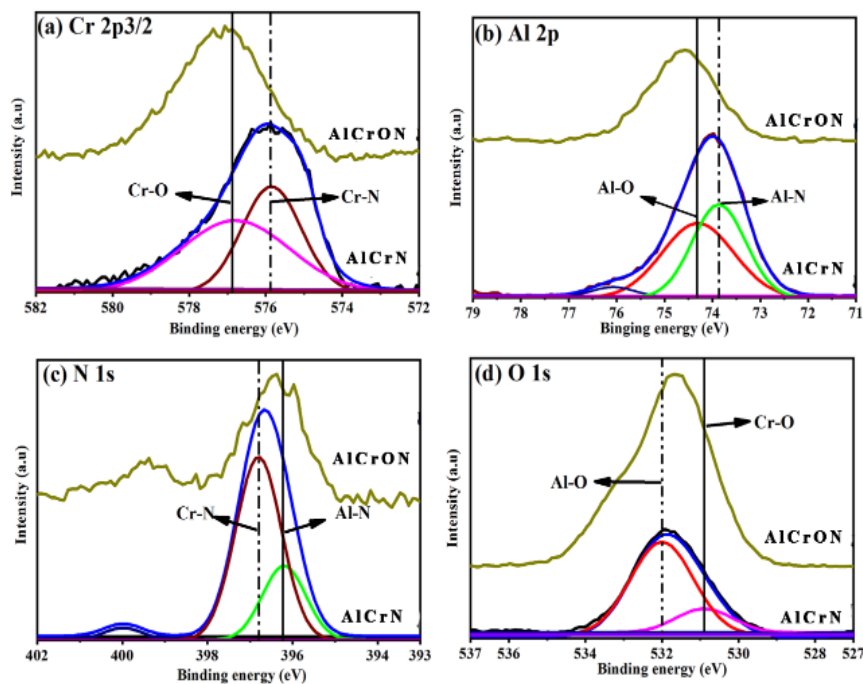
Figure 3. The XPS spectra of the AlCrN and AlCrON coatings: (**a**) Cr 2p3/2; (**b**) Al 2p; (**c**) N 1s; (**d**) O 1s.

Figure 4 presents typical cross-sectional TEM images of the as-deposited AlCrN/AlCrON coating. The columnar growth of the AlCrN base layer and AlCrON top layer can be observed in Figure 4a,b. The columnar gains are indicated by arrows while the interface between the nitride base layer and the oxynitride top layer is indicated with a dotted line. The cross-sectional selected area electron diffraction (SAED) analysis of AlCrON bilayered coating is shown in Figure 5. The spotty ring SAED pattern of the AlCrN layer shown in Figure 5a indicates the fine crystalline structure which grown in the preferred orientation [14]. Meanwhile, the SAED pattern analysis confirms the presence of fcc-CrN (JCPDS# 11 0065) and c-AlN (JCPDS# 46-1200) [28]. The SAED pattern of AlCrN base layer shows that (111), (200), (220), and (311) low-intensity rings are consistent with its X-ray diffraction pattern shown in Figure 2. The SAED pattern of AlCrON top layer shows distinct spots with reflections from

similar planes in Figure 5b. Khatibi et al. [28] reported that the fcc lattice in the AlCrON coating could withstand a large fraction of structural defects and vacancies, exhibiting the transformation of cubic to α-(Cr, Al)$_2$O$_3$ phase's structure with increasing oxygen content [28]. Najafi et al. [34] suggested the formation of a substitutional AlCr(O$_x$N$_{1-x}$) ($x < 0.6$) solid solution containing metal vacancies without any oxide segregation. Moreover, the intensity of (111) was sensitive to oxygen content. They found the circular sports diffused into amorphous rings of the fcc structure deposited by a cathodic arc deposition system. In this work, the SAED pattern of the AlCrON layer shows the B1 NaCl structure with (111), (200), (220), and (311) diffraction rings, confirming the formation of fcc-(Cr, Al)ON structure.
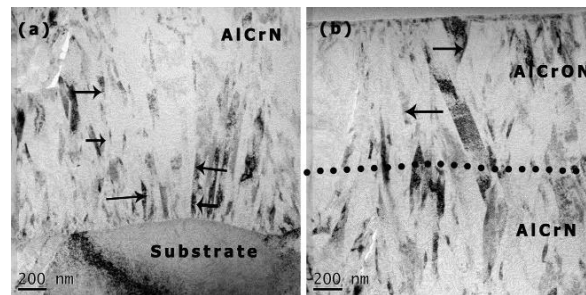
Figure 4. The cross-sectional TEM images of the AlCrON coating: (**a**) AlCrN base layer; (**b**) AlCrON top layer.
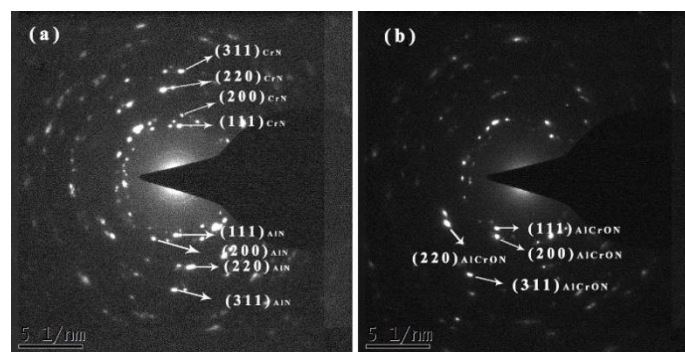
Figure 5. The SAED patterns of the AlCrON coating: (**a**) AlCrN base layer; (**b**) AlCrON top layer.

3.3. Mechanical Properties

The surface hardnessvalues and elastic moduli of duplex coatings are shown in Figure 6. It was found that the hardness (30.5 ± 1.5 GPa) and elastic modulus (339.8 ± 9.8 GPa) of AlCrN coating are higher than the hardness (28.6 ± 0.8 GPa) and elastic modulus (305.7 ± 6.3 GPa) of AlCrON bilayered coating. The addition of oxygen into the AlCrN coating considerably influences the hardness and elastic modulus of the coating. Due to the smaller ratio of anion vacancies or solid solution strengthing effect, the hadness would increase by doping a small amount of oxygen, while there is a progressive decrease of hardness with increasing oxygent content [35]. Actually, the compositions of the coatings have a significant influence on the hardness, including Cr and Al contents [14,28]. The replacement of anion from nitrogen to oxygen in the fcc structure changed the bonding position from covalence to a superior ionic bond, which resulted in a decrease of both hardness and elastic modulus [15,36]. In this study, the reduced hardness and elastic modulus of AlCrN/ACrON coating deposited by Al$_{70}$Cr$_{30}$ targets is attributed to the decrease in nitride bonding fraction, as evident from the XPS results.
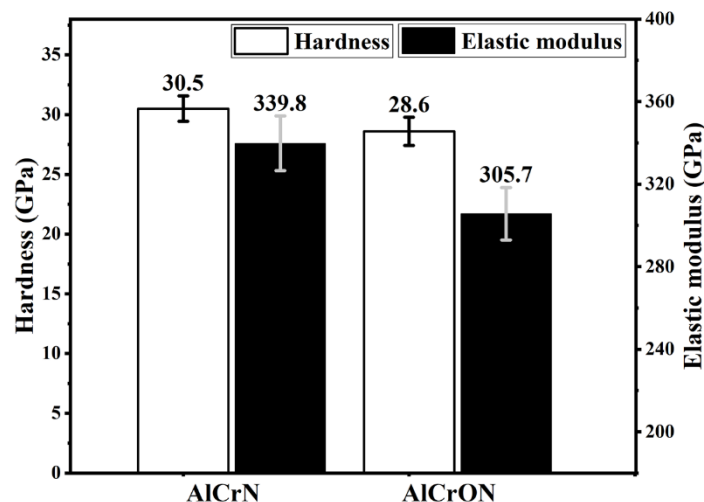
Figure 6. Surface hardness values and elastic moduli of AlCrN and AlCrON duplex coatings.

3.4. Thermal Stability

Figure 7 presents the XRD spectra of the AlCrN and AlCrON coatings after annealing at 700 °C for six hours. The fcc-(Cr, Al)N and fcc-(Cr, Al)ON solid solution phase were present in as-deposited AlCrN and AlCrN/AlCrON coatings respectively, and the diffraction peaks from the base layer contributed to the diffraction spectra of the top layer in oxynitride coatings. The XRD pattern of heat-treated AlCrON coating, compared with as-deposited coating, shows no obvious variation, while the shift of (200) diffraction peaks toward a higher angle can be related to release in the residual stress of coatings. The fcc-(Cr, Al)N phase of AlCrN coating slightly decomposed into bcc-Cr and h-Cr_2N phases by spinodal mechanism, which is evident from weak peaks at 2θ ≈ 65° and 40.15° respectively. The phase transformation of CrN into h-Cr_2N and bcc-Cr is caused by the deficiency of N resulting from precipitation of w-AlN at high temperatures [17]. The precipitation of w-AlN (at 2θ ≈ 36.1°) and formation of the hcp-Cr_2N phase at 700 °C can be related to the longer annealing time (i.e., 6 h). The lower intensity peaks of the hcp phase indicate the AlCrN coating consists mainly of the fcc-solid solution phase after annealing.
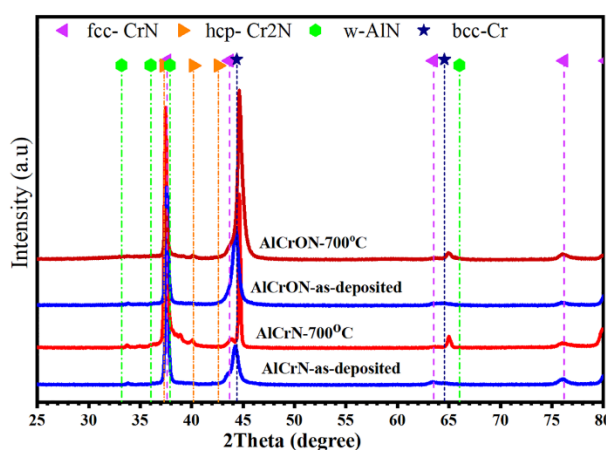
Figure 7. XRD patterns of the AlCrN and AlCrON coatings samples after annealing at 700 °C for 6 h.

The microstructural stabilities of AlCrN and AlCrON coatings were also compared using Raman spectroscopy. Figure 8 shows the Raman spectra of AlCrN and AlCrON coatings recorded subsequent to annealing and as-deposited samples. Raman spectra confirm the fcc-structure as reported elsewhere [37]. The fcc structure shows two Raman bands at 260 and 750 cm^{-1}. The band at 260 cm^{-1} corresponding to the lower frequency, indicates the fcc structure's vibrational acoustics, and the higher frequency band,

750 cm^{-1}, relates to that of vibrational optics modes [33,37]. Rather than a vibrational band, there are no other peaks observed, indicating that these coatings are thermally stable up to 700 °C. The XRD and Raman spectral analysis of the coatings after annealing verify that both AlCrN and AlCrON coatings are thermally stable at 700 °C. The thermal stability of AlCrON coating was improved with the introduction of oxygen, which can be related to the formation of the passive oxide layer (confirmed from XPS analysis) improving the oxidation resistance of AlCrN/AlCrON bilayered coating.
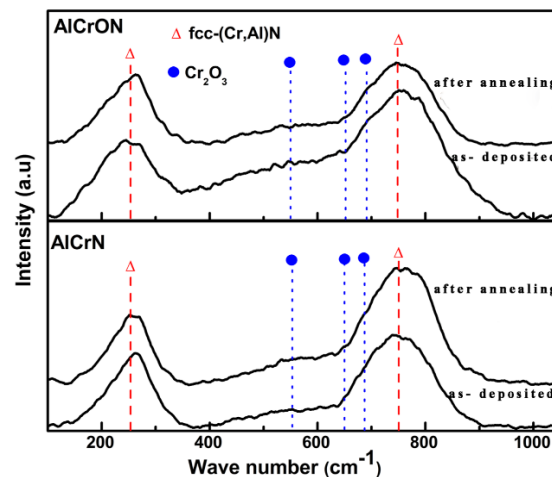
Figure 8. Raman spectra of the AlCrN and AlCrON coatings after annealing at 700 °C for 6 h.

The adhesion strength of the coating is essential and can affect the lifetime of the coating. A Rockwell indentation test was performed to determine coating's adhesion strength. The adhesion strengths of coatings were measured for as-deposited and annealed samples, and the adhesion of both coatings for the as-deposited sample was good. Figure 9 shows the SEM image of Rockwell indentation of coatings deposited on plasma nitride substrate after annealing at 700 °C. It can be seen from Figure 9a that the AlCrN coated sample has many cracks and a spalling zone at the indentation impress and interface of the coating, indicating that the adhesion is relatively low. Figure 9b shows the AlCrON coating has no spalling zone and fewer radial cracks on the interface, which was due to the compressive stress generated by the indentation. Based on these measurements, AlCrON and AlCrN coatings deposited on plasma nitrided steels exhibited excellent adhesion (HF1) and good adhesion (HF2) respectively [38].
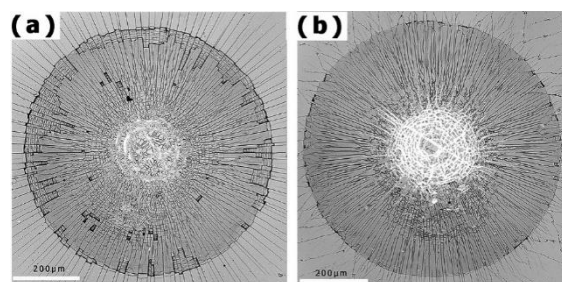
Figure 9. The SEM images of Rockwell indentation after annealing: (**a**) AlCrN coating; (**b**) AlCrON coating.

3.5. Tribological Properties

The wear resistance of hard protective coatings is usually characterized as a function of the coefficient of friction(CoF), hardness, and adhesion of the coating to the specimen. Figure 10a shows the friction coefficient evaluated at RT (room temperature). The friction coefficient of AlCrN coating increased firstly before 600 s as a result of contact stress variations and roughness of the surface;

after that, a steady-state reduced coefficient of friction was applied [39]. The decrease in friction coefficient before reaching a stable value is possibly related to wear out of particles or pits on the contacted surface. Figure 10b shows the evolution of friction coefficient curves at 600 °C during ball-on-disk tribological tests. It presents abrupt changes in CoF of AlCrN and AlCrON coatings at 600 °C, while it was stable at RT. The CoF analysis shows the significant wear damage to 600 °C for both coatings.
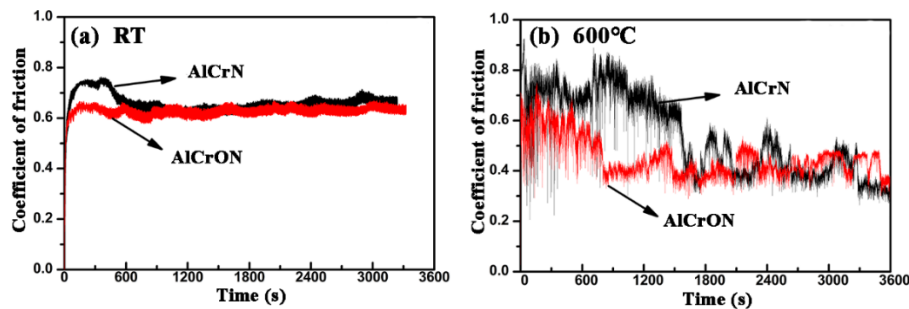
Figure 10. The CoF (coefficient of friction) against an Al_2O_3 ball for AlCrN and AlCrON coatings at (**a**) room temperature; (**b**) 600 °C.

The SEM examination of worn surface specimens is shown in Figure 11. The duplex coatings do not wear out, and the friction coefficient shows a constant value after RT wear test [24]. In Figure 11a,b, the smooth wear surface of coatings that is a typical feature of abrasive wear is shown. However, the wear track on the coatings after high temperature (600 °C) wear test, shows significant wear damage and build-up wear as illustrated in Figure 11c,d. The tribo-oxide delamination on the wear track of AlCrN and AlCrON coatings is presented in a magnified image view in Figure 11c,d. It causes the sudden variation in CoF of both coatings during high-temperature wear test. The oxidative wear in high temperature and dry sliding wear conditions is prominent from the literature [24,40]. The thermal softening, plastic deformation, and catastrophic adhesion failure can also contribute to mild wear to severe wear with elevated temperature. The additional cracks can also be observed on the wear track of AlCrN coating, which can be related to the catastrophic adhesion failure. The wear debris particles are measured up to 2 μm, indicating that wear debris also comes from typical particle ejection from the surface [40]. The EDS analysis of the wear track indicated in the Figure 11 shows the Cr content significantly reduced. This can be related to the presence of abrasive wear debris of the Al_2O_3 counterpart used for the wear test.

Figure 12b shows the 3D wear tracks on the coating surface after the wear test at room temperature. Only a small wear track is visible due to polishing wear in both coatings. The small peaks and valleys observed on the surface indicate the abrasive wear debris on the surface. A deep wear track can be observed in Figure 12c,d which indicates severe wear of coating after wear test conducted at 600 °C in the ambient atmosphere. The shallower wear track on the AlCrON bilayered coating surface than that of AlCrN coating indicated an improved wear resistance of the coating at high temperature with the introduction of oxygen. Moreover, the low wear of AlCrN and AlCrON coatings at RT was followed by complete abrasion wear at 600 °C. The significant reduction in adhesion and hardness can be attributed to increased operating temperature [40]. Meanwhile, the wear rates of both coatings have been compared in Table 1. The wear rates are almost non-measurable at room temperature, which shows the excellent wear properties of both coatings, which is similar to other reports [24,41]. The increased wear volume at high temperatures is attributed to the delamination of thick tribo-oxide layers through the evolved friction mentioned above. The reduction in friction could have resulted from the presence of oxides in the tribolayer [42]. However, a direct relationship between wear rates and the temperature is common for CrN-based coatings [41]. Table 1 shows that both the AlCrN and AlCrON coatings exhibit maximum wear rates of 4.5×10^{-16} and 2.7×10^{-16} m³/(N·m) under dry conditions, respectively. Several studies reported the wear resistance of AlCrN coating deposited with various techniques

under different testing conditions regarding the different coating applications [43–45]. The reasonable wear resistance at 600 °C was observed in cubic AlCrN and AlCrON coatings, and oxynitride coating exhibited improving wear resistance due to the high ability of a coating to resist oxidation and to delay substrate oxidation [24]. In this work, although the as-deposited AlCrON bilayered coating presents dense structure and excellent thermal stability, both coatings exhibited severe wear at the evaluated temperature. That could be attributed to the low thicknesses of the coatings. When the thin AlCrON coating failed, the coating would wear out rapidly. Based on the above results, the AlCrN/AlCrON bilayered coating with the fcc-AlCrON structure presents better tribological performance compared to the AlCrN coating, making it a suitable candidate for the HPDC application. The thick AlCrON coatings with optimal properties will be investigated systematically in future.
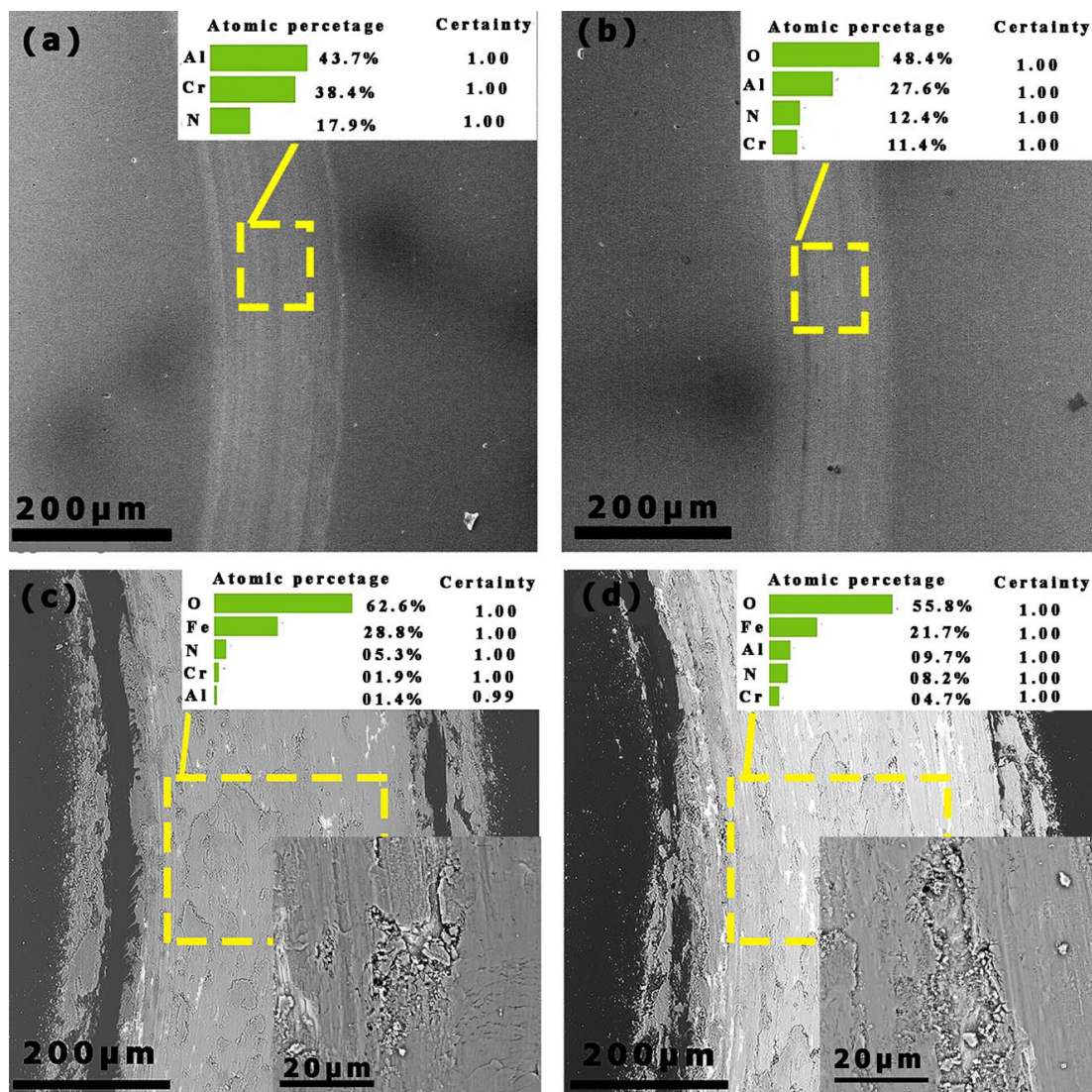
Figure 11. Wear track of the duplex coatings. (**a**) AlCrN at RT; (**b**) AlCrON at RT; (**c**) AlCrN at 600 °C; and (**d**) AlCrON at 600 °C.
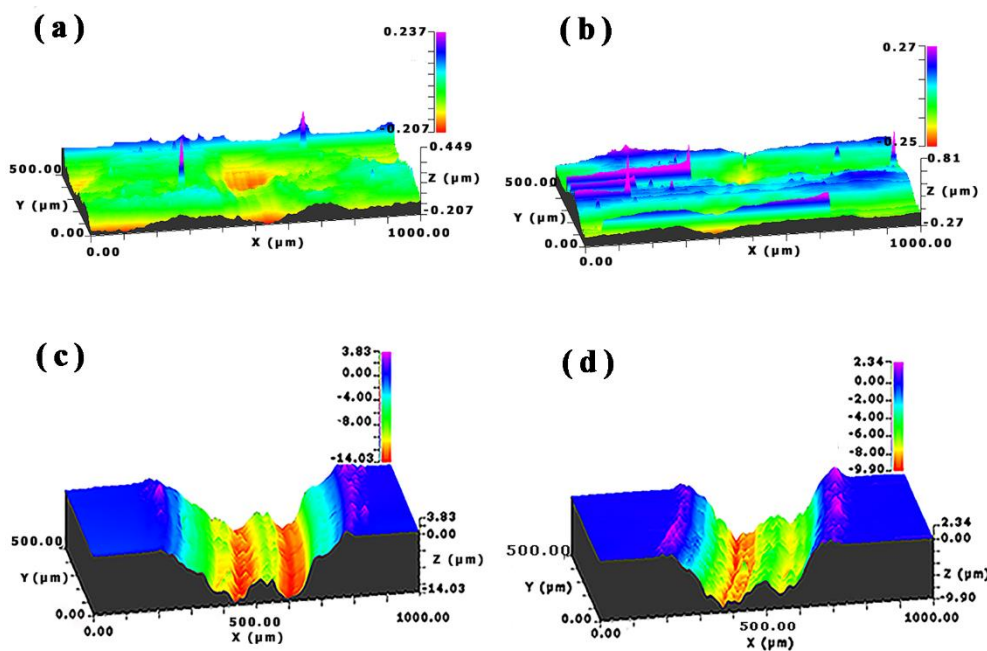
Figure 12. The 3D wear scar step profiler images of the duplex coatings (**a**) AlCrN at RT; (**b**) AlCrON at RT; (**c**) AlCrN at 600 °C; and (**d**) AlCrON at 600 °C.

Table 1. The wear rate of the AlCrN and AlCrON coated samples at room temperature and 600 °C.

Coatings	Wear Rate-RT $\times 10^{-18}$ (m³/(N·m))	Wear Rate-600 °C $\times 10^{-16}$ (m³/(N·m))
AlCrN	0.98 ± 0.02	4.5 ± 0.42
AlCrN/AlCrON	0.77 ± 0.01	2.7 ± 0.36

4. Conclusions

AlCrN and AlCrN/AlCrON duplex coatings were prepared on plasma nitrided-AISI H13 tool steels by ion-source-enhanced arc ion plating. The AlCrN coating was deposited in pure N_2 while AlCrON the top layer was deposited under the O_2/N_2 flow ratio of 1:10. The as-deposited AlCrN and AlCrON bilayered coatings consisted of solid solution fcc-AlCrN and fcc-AlCrON crystallites respectively. The AlCrON bilayered coating showed higher surface roughness than that of AlCrN coating. The hardness and elastic modulus of AlCrN coating decreased with the addition of a thin AlCrON layer. The AlCrON bilayered coating exhibited good thermal stability after annealing at 700 °C. Both coatings present excellent wear resistance at room temperature, while at 600 °C the severe abrasive and oxidation wear mechanism against Al_2O_3 ball was observed. The AlCrON bilayered coating showed better wear resistance in comparison with AlCrN coating, which was related to its high adhesion strength and thermal stability resulting from the effect of dense AlCrON layer.

Author Contributions: Manuscript writing, carrying out experiments, data analysis, F.A.; study design, L.Z.; experimental guidance, J.Z.; literature search, I.S.; project administration, S.Z. All authors have read and agreed to the published version of the manuscript.

Funding: This research was supported by the Project of Anhui Provincial Key Research and Development Program (grant number 1804b06020370).

Conflicts of Interest: The authors declare no conflict of interest.

References

1. Chen, Z.; Jahedi, M. Die erosion and its effect on soldering formation in high pressure die casting of aluminium alloys. *Mater. Des.* **1999**, *20*, 303–309. [CrossRef]

2. Cundari, T. *Experimental Study about Thermal Fatigue and Erosion Failures on HPDC Dies*; Universita' Degli Studi di Padova: Padova, Italy, 2016.

3. Dasaratha Prabhu, B.; Ramesh Babu, K. Investigating the significance of parameters affecting the defects in HPDC component using design of experiment method. *IOSR J. Environ. Sci. Toxicol. Food Technol.* **2013**, *4*, 4–9. [CrossRef]

4. Soković, M.; Panjan, P.; Kim, R. Possibilities of improvement of dies casting tools with duplex treatment. *Proc. J. Mater. Process. Technol.* **2004**, *157–158*, 613–616. [CrossRef]

5. Navinšek, B.; Panjan, P.; Gorenjak, F. Improvement of hot forging manufacturing with PVD and DUPLEX coatings. *Surf. Coat. Technol.* **2001**, *137*, 255–264. [CrossRef]

6. Jerina, J.; Kalin, M. Aluminium-alloy transfer to a CrN coating and a hot-work tool steel at room and elevated temperatures. *Wear* **2014**, *340–341*, 82–89. [CrossRef]

7. Mitterer, C.; Holler, F.; Üstel, F.; Heim, D. Application of hard coatings in aluminium die casting—Soldering, erosion and thermal fatigue behaviour. *Surf. Coat. Technol.* **2000**, *125*, 233–239. [CrossRef]

8. Birol, Y. Sliding wear of CrN, AlCrN and AlTiN coated AISI H13 hot work tool steels in aluminium extrusion. *Tribol. Int.* **2013**, *57*, 101–106. [CrossRef]

9. Bobzin, K.; Brögelmann, T.; Hartmann, U.; Kruppe, N.C. Analysis of $CrN/AlN/Al_2O_3$ and two industrially used coatings deposited on die casting cores after application in an aluminum die casting machine. *Surf. Coat. Technol.* **2016**, *308*, 374–382. [CrossRef]

10. Cha, S.C.; Erdemir, A. Coatings for Aluminum Die-Casting Dies. In *Coating Technology for Vehicle Applications*; Springer International Publishing: Basel, Switzerland, 2015; pp. 163–175.

11. Xiao, B.; Li, H.; Mei, H.; Dai, W.; Zuo, F.; Wu, Z.; Wang, Q. A study of oxidation behavior of AlTiN-and AlCrN-based multilayer coatings. *Surf. Coat. Technol.* **2018**, *333*, 229–237. [CrossRef]

12. Ho, W.Y.; Hsu, P.H.; Lin, C.L. Characteristics of aluminum chromium nitride, and aluminum chromium oxynitride coating through cathodic arc deposition. *Key Eng. Mater.* **2017**, *735*, 70–74. [CrossRef]

13. Chen, W.; Zheng, J.; Meng, X.; Kwon, S.; Zhang, S. Investigation on microstructures and mechanical properties of AlCrN coatings deposited on the surface of plasma nitrocarburized cool-work tool steels. *Vacuum* **2015**, *121*, 194–201. [CrossRef]

14. Stüber, M.; Albers, U.; Leiste, H.; Seemann, K.; Ziebert, C.; Ulrich, S. Magnetron sputtering of hard Cr-Al-N-O thin films. *Surf. Coat. Technol.* **2008**, *203*, 661–665. [CrossRef]

15. Najafi, H.; Karimi, A.; Dessarzin, P.; Morstein, M. Correlation between anionic substitution and structural properties in $AlCr(O_xN_{1-x})$ coatings deposited by lateral rotating cathode arc PVD. *Thin Solid Film.* **2011**, *520*, 1597–1602. [CrossRef]

16. Bobzin, K.; Brögelmann, T.; Kalscheuer, C.; Naderi, M. Hybrid dcMS/HPPMS PVD nitride and oxynitride hard coatings for adhesion and abrasion reduction in plastics processing. *Surf. Coat. Technol.* **2016**, *308*, 349–359. [CrossRef]

17. Bobzin, K.; Brögelmann, T.; Kalscheuer, C.; Liang, T. High temperature oxidation protection of γ-titanium aluminide using (Cr, Al)ON coatings deposited by high-speed physical vapor deposition. *Surf. Coat. Technol.* **2017**, *332*, 2–11. [CrossRef]

18. Bobzin, K.; Brögelmann, T.; Grundmeier, G.; de los Arcos, T.; Wiesing, M.; Kruppe, N.C. (Cr, Al)N/(Cr, Al)ON Oxy-nitride Coatings deposited by Hybrid dcMS/HPPMS for Plastics Processing Applications. *Surf. Coat. Technol.* **2016**, *308*, 394–403. [CrossRef]

19. Pilkington, A.; Dowey, S.J.; Toton, J.T.; Doyle, E.D. Machining with AlCr-oxinitride PVD coated cutting tools. *Tribol. Int.* **2013**, *65*, 303–313. [CrossRef]

20. Veprek, S.; Veprek-Heijman, M.J.G. Industrial applications of superhard nanocomposite coatings. *Surf. Coat. Technol.* **2008**, *202*, 5063–5073. [CrossRef]

21. Veprek, S.; Zhang, R.F.; Veprek-Heijman, M.G.J.; Sheng, S.H.; Argon, A.S. Superhard nanocomposites: Origin of hardness enhancement, properties and applications. *Surf. Coat. Technol.* **2010**, *204*, 1898–1906. [CrossRef]

22. Bagcivan, N.; Bobzin, K.; Brögelmann, T.; Kalscheuer, C. Development of (Cr, Al)ON coatings using middle frequency magnetron sputtering and investigations on tribological behavior against polymers. *Surf. Coat. Technol.* **2014**, *260*, 347–361. [CrossRef]

23. Brögelmann, T.; Bobzin, K.; Kruppe, N.C.; Arghavani, M. Investigation on the influence of oxygen on the deformation and cracking behavior of (Cr, Al)ON hard coatings using combinatorial static and dynamic loadings. *J. Vac. Sci. Technol. A* **2019**, *37*, 061509. [CrossRef]

24. Nohava, J.; Dessarzin, P.; Karvankova, P.; Morstein, M. Characterization of tribological behavior and wear mechanisms of novel oxynitride PVD coatings designed for applications at high temperatures. *Tribol. Int.* **2015**, *81*, 231–239. [CrossRef]

25. Anders, A. A review comparing cathodic arcs and high power impulse magnetron sputtering (HiPIMS). *Surf. Coat. Technol.* **2014**, *257*, 308–325. [CrossRef]

26. Cai, F.; Gao, Y.; Fang, W.; Mao, T.; Zhang, S.H.; Wang, Q.M. Improved adhesion and cutting performance of AlTiSiN coatings by tuning substrate bias voltage combined with Ar ion cleaning pre-treatment. *Ceram. Int.* **2018**, *44*, 18894–18902. [CrossRef]

27. Qi, D.; Lei, H.; Wang, T.; Pei, Z.; Gong, J.; Sun, C. Mechanical, Microstructural and Tribological Properties of Reactive Magnetron Sputtered Cr-Mo-N Films. *J. Mater. Sci. Technol.* **2015**, *31*, 55–64. [CrossRef]

28. Khatibi, A.; Sjölen, J.; Greczynski, G.; Jensen, J.; Eklund, P.; Hultman, L. Structural and mechanical properties of Cr-Al-O-N thin films grown by cathodic arc deposition. *Acta Mater.* **2012**, *60*, 6494–6507. [CrossRef]

29. Castaldi, L.; Kurapov, D.; Reiter, A.; Shklover, V.; Schwaller, P.; Patscheider, J. Effect of the oxygen content on the structure, morphology and oxidation resistance of Cr-O-N coatings. *Surf. Coat. Technol.* **2008**, *203*, 545–549. [CrossRef]

30. Bobzin, K.; Brögelmann, T.; Kruppe, N.C.; Arghavani, M.; Mayer, J.; Weirich, T.E. On the plastic deformation of chromium-based nitride hard coatings deposited by hybrid dcMS/HPPMS: A fundamental study using nanoscratch test. *Surf. Coat. Technol.* **2016**, *308*, 298–306. [CrossRef]

31. Geng, D.; Li, H.; Zhang, Q.; Zhang, X.; Wang, C.; Wu, Z.; Wang, Q. Effect of incorporating oxygen on microstructure and mechanical properties of AlCrSiON coatings deposited by arc ion plating. *Surf. Coat. Technol.* **2017**, *310*, 223–230. [CrossRef]

32. NIST Standard References Data (SRD). Available online: https://srdata.nist.gov/xps/selEnergyType.aspx (accessed on 11 January 2020).

33. Barshilia, H.C.; Deepthi, B.; Selvakumar, N.; Jain, A.; Rajam, K.S. Nanolayered multilayer coatings of CrN/CrAlN prepared by reactive DC magnetron sputtering. *Appl. Surf. Sci.* **2007**, *253*, 5076–5083. [CrossRef]

34. Najafi, H.; Karimi, A.; Oveisi, E.; Morstein, M. Structure and electronic properties of AlCrO$_X$N$_{1-X}$ thin films deposited by reactive magnetron sputtering. *Thin Solid Film.* **2014**, *572*, 176–183. [CrossRef]

35. Almandoz, E.; Fuentes, G.G.; Fernández, J.; de Bujanda, J.M.; Rodríguez, R.J.; Pérez-Trujillo, F.J.; Alcalá, G.; Lousa, A.; Qin, Y. Chemical and mechanical stability of air annealed cathodic arc evaporated CrAlON coatings. *Surf. Coat. Technol.* **2018**, *351*, 153–161. [CrossRef]

36. Shaha, K.P.; Rueß, H.; Rotert, S.; To Baben, M.; Music, D.; Schneider, J.M. Nonmetal sublattice population induced defect structure in transition metal aluminum oxynitrides. *Appl. Phys. Lett.* **2013**, *103*, 1–6. [CrossRef]

37. Soldán, J.; Neidhardt, J.; Sartory, B.; Kaindl, R.; Čerstvý, R.; Mayrhofer, P.H.; Tessadri, R.; Polcik, P.; Lechthaler, M.; Mitterer, C. Structure-property relations of arc-evaporated Al-Cr-Si-N coatings. *Surf. Coat. Technol.* **2008**, *202*, 3555–3562. [CrossRef]

38. Haršáni, M.; Ghafoor, N.; Calamba, K.; Zacková, P.; Sahul, M.; Vopát, T.; Satrapinskyy, L.; Čaplovičová, M. Čaplovič Adhesive-deformation relationships and mechanical properties of nc-AlCrN/a-SiNx hard coatings deposited at different bias voltages. *Thin Solid Film.* **2018**, *650*, 11–19. [CrossRef]

39. Panjan, P.; Drnovšek, A.; Kovač, J. Tribological aspects related to the morphology of PVD hard coatings. *Surf. Coat. Technol.* **2018**, *343*, 138–147. [CrossRef]

40. Polcar, T.; Cavaleiro, A. High-temperature tribological properties of CrAlN, CrAlSiN and AlCrSiN coatings. *Surf. Coat. Technol.* **2011**, *206*, 1244–1251. [CrossRef]

41. Polcar, T.; Cavaleiro, A. High temperature properties of CrAlN, CrAlSiN and AlCrSiN coatings—Structure and oxidation. *Mater. Chem. Phys.* **2011**, *129*, 195–201. [CrossRef]

42. Polcar, T.; Parreira, N.M.G.; Novák, R. Friction and wear behaviour of CrN coating at temperatures up to 500 °C. *Surf. Coat. Technol.* **2007**, *201*, 5228–5235. [CrossRef]

43. Adesina, A.Y.; Gasem, Z.M.; Mohammed, A.S. Comparative Investigation and Characterization of the Scratch and Wear Resistance Behavior of TiN, CrN, AlTiN and AlCrN Cathodic Arc PVD Coatings. *Arab. J. Sci. Eng.* **2019**, *44*, 10355–10371. [CrossRef]

44. Souza, P.S.; Santos, A.J.; Cotrim, M.A.P.; Abrão, A.M.; Câmara, M.A. Analysis of the surface energy interactions in the tribological behavior of AlCrN and TiAlN coatings. *Tribol. Int.* **2020**, *146*, 106206. [CrossRef]

45. Antonov, M.; Afshari, H.; Baronins, J.; Adoberg, E.; Raadik, T.; Hussainova, I. The effect of temperature and sliding speed on friction and wear of Si_3N_4, Al_2O_3, and ZrO_2 balls tested against AlCrN PVD coating. *Tribol. Int.* **2018**, *118*, 500–514. [CrossRef]